The MU2E experiment at Fermilab

G.Bisogni(Asso.Senior), P.Ciambrone, F.Colao (Asso.), M.Cordelli, E.Dane'(Art.23), E.Diociaiuti(Dott.), R.Donghia(Dott.), F.Fontana (Asso.), S.Giovannella, F.Happacher, M.Martini (Asso.), A.Mengucci(Tech), S.Miscetti (Resp), B.Ponzio(Tech), G.Pileggi(Tech), M.Ricci(AR), A.Saputi(Tech), I.Sarra(AR), M. Ventura (Tech).
In collaboration with LNF-SEA: G.Corradi, S.Ceravolo

1 Introduction

During 2016, Mu2e has achieved many important milestones such as the completion of the building for the experiment, the production of all superconducting cables, the start of the construction for the three large solenoids: the Production and the Detector solenoids have been assigned to the General Atomics, in USA, while the Transport solenoid has been assigned to AGS superconducting in Genova. In the mean time, the Mu2e LNF group participated to many reviews at Fermilab (Final Design Review, Independent Design Review) in preparation for the final DOE review (CD-3c) to obtain the green light for the calorimeter construction. CD-3c was granted by DOE in July 2016. Soon after, the INFN approval was also received with the signature of the Statement of Work with Fermilab for this construction. The Mu2e calorimeter design is now being refined and engineered to arrive to a final version for Construction Readiness at the end of 2017. The calorimeter consists of 2 disks of 674 un-doped parallelepiped CsI crystals of $(34\times34\times200)$ mm^3 dimension. Each crystal is readout by means of two custom large area, (12x18) mm^2, UV extended Silicon Photomultipliers (Mu2e SiPMs).

The most relevant items we have carried out during 2016 are reported in the next sessions and are summarized by the following list: (i) the start of the pre-production bids for crystals and sensors, (ii) the design of the pre-production FEE version and (iii) the engineering and prototyping of the mechanics. In order to proceed to the quality assurance, QA, of the pre-production, we have completed a long list of R&D items to better tune the QA tests for the characterisation of un-doped CsI crystals and Mu2e SiPMs.

2 Quality assurance of CsI crystals and crystal pre-production

At the end of 2015, the technical choice between BaF_2 and CsI crystals was completed and we have downselected un-doped CsI as the final crystal choice for the calorimeter. During 2016, we have completed the tests on the 16 CsI crystals received in 2015 from OptoMaterials (Italy), SICCAS (China) and ISMA/AMCRYS (Ukraine) companies and used this development for the QA, carried out at end of 2016, on 36 pre-production crystals. In particular, we have learnt how to determine the slow component on the scintillation decay time and the radiation induced noise, RIN, due to either the thermal neutrons or to dose by a gamma source.

2.1 CsI light emission decay time

The scintillation light of un-doped CsI crystals often presents two components: the fast one (315 nm) with a decay time, τ, of $\sim$ 30 ns and a slow one (>380 nm) with decay times between 600 ns to few μs. In general, this slow component is related to remaining impurities in the process of the crystal growth. We developed a precise measurement of these components and defined a tight specification on it for the production stage so to match the calorimeter requirements.

We have performed the measurement of the slow component for several $(30\times30\times200)$ mm^3 un-doped CsI crystals: 6 from SICCAS, 8 from ISMA and 2 from Opto Materials. All of them

have been tested at our crystal test station where a reference Na^{22} source was illuminating both the crystal under test, CUT, and a tag system provided by a small $(3 \times 3 \times 6)$ mm^3 LYSO crystal readout with a (3×3) mm^3 MPPC. The 511 keV annihilation photon provided our test probe. The CUT was readout by means of a UV extended PMT from EMI, coupled in air. Both tag and test crystal signals have been acquired with a CAEN DT5751 digitizer at 1 Gsps rate. All crystals have been wrapped with Tyvek foils. For one of the ISMA crystals, with same wrapping and readout system, the slow component has been also measured using cosmic ray events, selected by the coincidence of two $(6 \times 10 \times 50)$ mm^3 plastic scintillation counters read out by a (3×3) mm^2 silicon photomultipliers.

The fast and slow components have been extracted from the distribution of the Q_{INT}/Q_{TOT} variable as a function of $DT = T - T_{mean}$, with 20 ns bin width, where T is the digitizer time, T_{mean} is the time corresponding to the pulse height peak, Q_{INT} is the charge integrated from the start of the signal ($DT = -30$ ns) while Q_{TOT} is the charge integrated in the full range. This distribution is fit with the following function $f(x) = P_1 \cdot [1 - \exp(-x/\tau_1)] + P_2 \cdot [1 - \exp(-x/\tau_2)]$. The fit quality for SICCAS crystals is not good, suggesting that an additional component may be needed in the decay time parametrization. The fast component extracted from the fit has $\tau_1 \sim 35$ ns, while the slow one has a decay time, τ_2, between 700 and 3000 ns for five of the crystals.

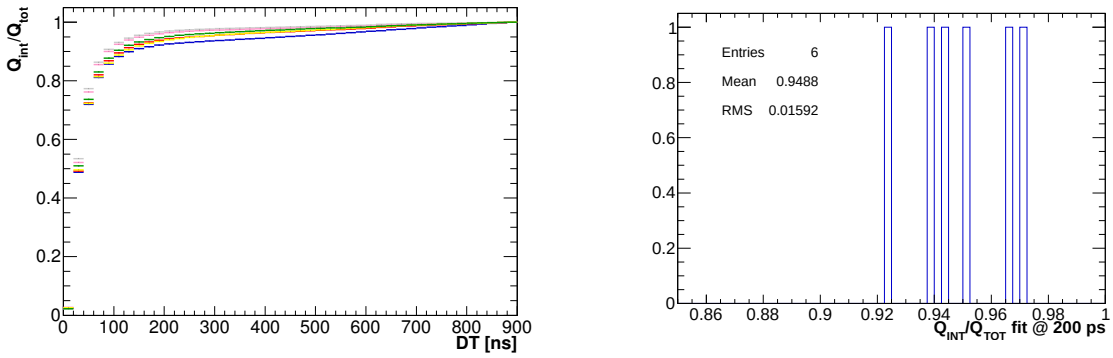

Figure 1: *Summary of the measurements obtained for all six SICCAS crystals:* Q_{int}/Q_{tot} *ratio as a function of DT (left) and distribution of fit results evaluated at 200 ns (right).*

In Fig. 1 left, the distribution of the Q_{INT}/Q_{TOT} ratio for all SICCAS crystals is reported, showing three different behaviours. The relative contribution of the fast/total component has been extracted by evaluating the fit function at DT = 200 ns, $f(200)$. The distribution of the $f(200)$values obtained for SICCAS crystals is reported in Fig. 1 right. The mean value of the six crystals is 94.9%, with 1.5% RMS. Fit results of the eight ISMA crystals showed a decay time of the fast component $\tau_1 \geq 30$ ns, while τ_2 ranged between $200 \div 1000$ ns. The mean time of their $f(200)$ values is of 92.7%, few per cent lower than that obtained for SICCAS crystals, with an RMS of 0.02. The resulting fraction of the fast component of the two Opto Materials crystals are 94.3% and 93.4%, respectively. The measurement repeated for one ISMA crystals using cosmic rays data, provided $f(200) = 93.3\%$ and the shape of the Q_{int}/Q_{tot} ratio is consistent with the ones obtained with the source runs.

As in literature, the fit results from all tested crystals have shown a fast component consistent with a decay time of $30 \div 35$ ns, while the slow component varied from 350 to 3500 ns.

2.2 Radiation Induced Noise for thermal neutrons and dose

An important issue, related to the Mu2e environment, is that of controlling the phosphorescence light induced by radiation and evaluate the corresponding equivalent energy noise when the crystals are exposed to an instantaneous fluency or a dose rate similar to the one expected while running in Mu2e.

In May 2016, the "2015" crystals have been tested with thermal neutrons at the HOTNES facility at ENEA-Frascati: a single crystal, coupled to a photomultiplier with a gain of 2.1×10^6 at 1400 V, has been inserted inside the Am-B source and thus irradiated with a uniform flux of 700 n/cm^2/s. The dark current values, Id, have been recorded by means of a Keythley picoammeter. To evaluate the RIN, we first determined F, which is the radiation induced number of photoelectrons/s/neutron flux, defined as: $F = \frac{Id}{e \times G_{PMT} \times \phi_N}$. We then considered an integration gate of 200 ns and an estimated flux of 10^4 n/cm^2/s, so that the number of expected photoelectrons in the gate can be derived as: $N_{p.e} = F \times \phi_{Mu2e} \times 200$ ns. Finally from this number, the RIN is obtained using the following relation:

$$RIN = \frac{\sqrt{N_{p.e.}}}{LY} \tag{1}$$

Results are reported in Table 1. In Figure 2, examples of the current seen from differente crystals when irradiated are shown.

Crystal	LY [N$_{p.e.}$/MeV]	I[μA]	F[N$_{p.e.}$/s/flux]	N$_{p.e.}$	RIN_{Mu2e} [keV]
ISMA 02	103	7.16	3.02×10^4	60.3	75.4
ISMA 12	103	4.61	1.94×10^4	38.9	60.5
ISMA 20	103	5.35	2.25×10^4	45.1	65.2
ISMA 21	103	7.28	3.07×10^4	61.4	76.0
SICCAS 1	129	6.83	2.88×10^4	57.5	58.6
SICCAS 2	126	7.58	3.19×10^4	63.8	63.4
SICCAS 4	136	10.1	4.27×10^4	85.5	67.8
OPTOM 2	93	7.65	3.22×10^4	64.4	86.3

Table 1: *Results from RIN test with thermal neutrons at HOTNES Facility.*

The value of the current increases from $I \sim 10$ nA, when the crystal is not irradiated, to $I_d \sim \mathcal{O}(10)$ μA during irradiation. All tested crystals showed a similar behaviour and the RIN values obtained, that is between 60-85 keV for a flux F=10^4 n/cm^2/s, is well inside the Mu2e requirement of a RIN$<$ 0.6 MeV.

We have also evaluated the RIN by gammas at LNF by exposing the same crystals to an intense ^{167}Co source, which emits 700 keV photons. Using the same formulas of the thermal neutron RIN study and considering a Mu2e flux of 1.8 rad/h we obtained a not negligible RIN. All the measurements are reported in Table 2. The expected RIN from γ-ray in the hottest Mu2e region is around 300 keV.

2.3 Tender for pre-production crystals

Following the experience done with the prototypes, a tight specification on all scintillation and mechanical parameters have been defined for pre-production and production QA as follows:

- High light output (LY) $>$ 100 p.e./MeV with PMT readout and air-coupling;
- Good light response uniformity (LRU): $<$ 5%;

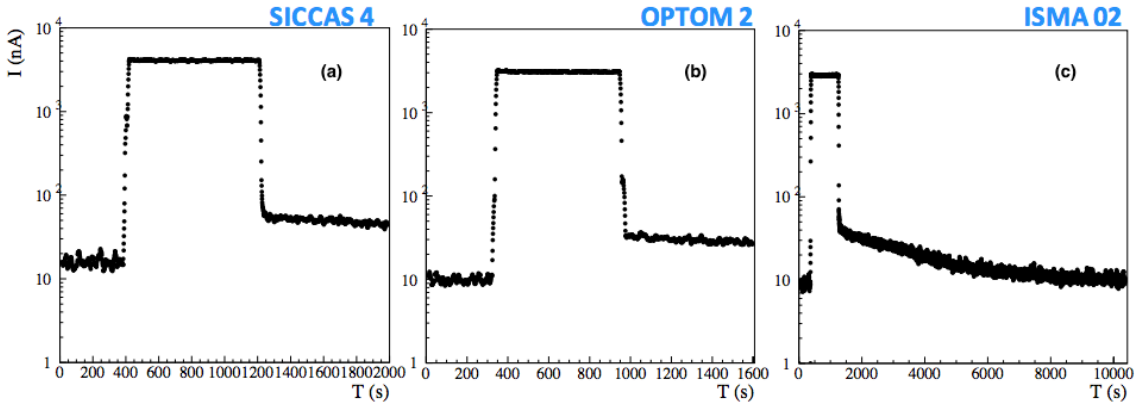

Figure 2: *Radiation induced current from SICCAS (a), OptoMaterials (b) and ISMA (c) crystals when exposed to a thermal neutron flux of* 700 n/cm^2/sec.

Crystal	LY [$N_{p.e.}$/MeV]	I[μA]	F[$N_{p.e.}$/s/flux]	$N_{p.e.}$	RIN_{Mu2e} [keV]
ISMA 01	103	157	2.31×10^9	845	283
ISMA 02	103	215	3.17×10^9	1160	331
SICCAS 1	129	188	2.77×10^9	1010	226
SICCAS 2	126	160	2.36×10^9	861	233
SICCAS 4	136	157	2.31×10^9	845	213
OPTOM 2	93	187	2.76×10^9	1010	341

Table 2: *Results from RIN test with the* ^{167}*Co source.*

- Good energy resolution at 511 keV, $\sigma_E/E < 19$ %;
- Fast signal with small slow component: $\tau < 40$ ns, F/T > 75%;
- Radiation hardness with LY loss < 40% (for ionization dose ~ 100 krad and neutron fluency up to 10^{12} n/cm^2);
- RIN < 0.6 MeV.

During the 2016, the bid to define the final crystal vendor is started. The participating companies are: Saint Gobain, SICCAS and Amcrys. We received 24 crystals per vendor. Their mechanical shapes and dimensions have been first controlled at Femilab. Then 12 crystals/each vendor have been sent both to LNF and Caltech.

2.4 Survey of mechanical characteristics of Pre-production crystals

After having been visually inspected, each crystal has been measured with a Coordinate Measuring Machine (CMM), for a total of 112 points acquired: 20 on each long face and 16 on each square small face. Starting from these measurements the flatness of every face as well as their perpendicularity and parallelism have been obtained. The aim of this first test was to guarantee that the different vendors had respected the required dimensional specifications such as a cross-sectional dimension between 33.9 mm and 40.1 mm. We have also required a tolerance of $\pm$ 0.1 mm on the crystal length and a flatness, parallelism and perpendicularity lower than 0.1 mm. Results of the measurements are reported in Figure 3.

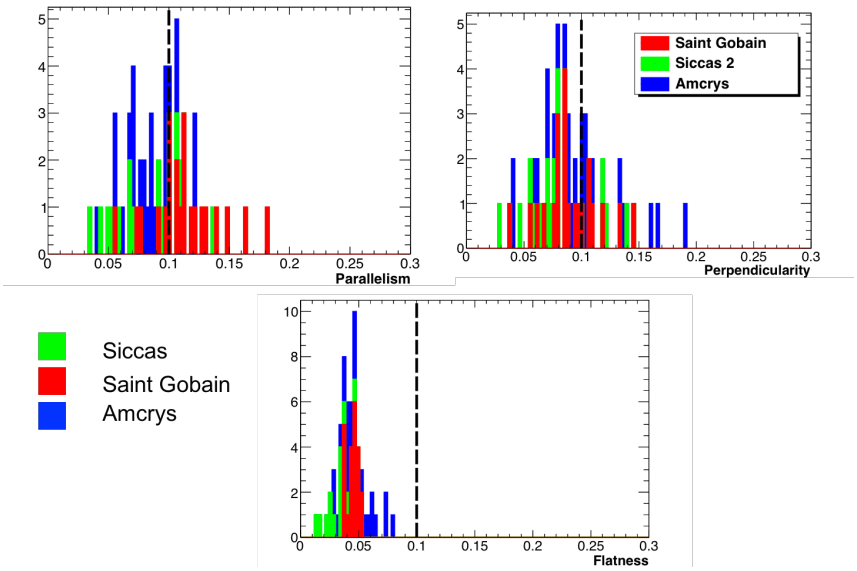

Figure 3: *Summary of the shape tolerances for the 72 pre-production crystals.*

2.5 Survey of Scintillation properties of pre-production crystals

The scintillation properties have been evaluated for all the pre-production sample. The results are reported in Fig. 4.

The light yield (LY) have been obtained integrating the signal shape in a fixed window of 200 ns around the pulse height maximum. This integration takes into account most of the fast emission component. This is shown in the Top-left plot. All crystals well exceed the specifications. In the Top-right plot, the Longitudinal Response Uniformity, LRU, is shown. This is defined as the RMS of the LY, which has been measured in 8 different positions of the source with respect to the readout system. The LRU is pretty good and better than the required 5%. All the crystals satisfy this requirement, except for four SICCAS and 1 St.Gobain crystals. In the Bottom-left plot, the distribution of energy resolution at 511 keV is shown. The average is 14.5% that is more than satisfying. Finally, in the Bottom-right plot the distribution of the F/T ratio in a 900 ns gate is shown. The measurements in a 3 μs gate is under way at the moment of writing.

3 The Mu2e SiPMs

Each crystal is read by two 2×3 arrays of individual (6×6) mm ^{2} UV-extended SiPMs, see Fig. 5. The solid-state photodetectors are necessary due to the presence of a high magnetic field while the choice of UV-extended sensitivity allows to match the wavelength of the emitted light produced by the CsI crystals (that is centered at 315 nm).

The configuration in serial connection has been selected to overcome the issues related to the parallel connection which might affect the energy and time measurements, owing to the very large capacitance. This is shown in Fig. 6, where the signal width of a single SiPM and the series of three SiPMs are reported. Differently from the parallel configuration, where the signal becomes wider, the pulse shape of a series of SiPMs results narrower than the one of a single SiPM. This is due to the reduction of the total capacitance of the circuit. The shorter signal decay

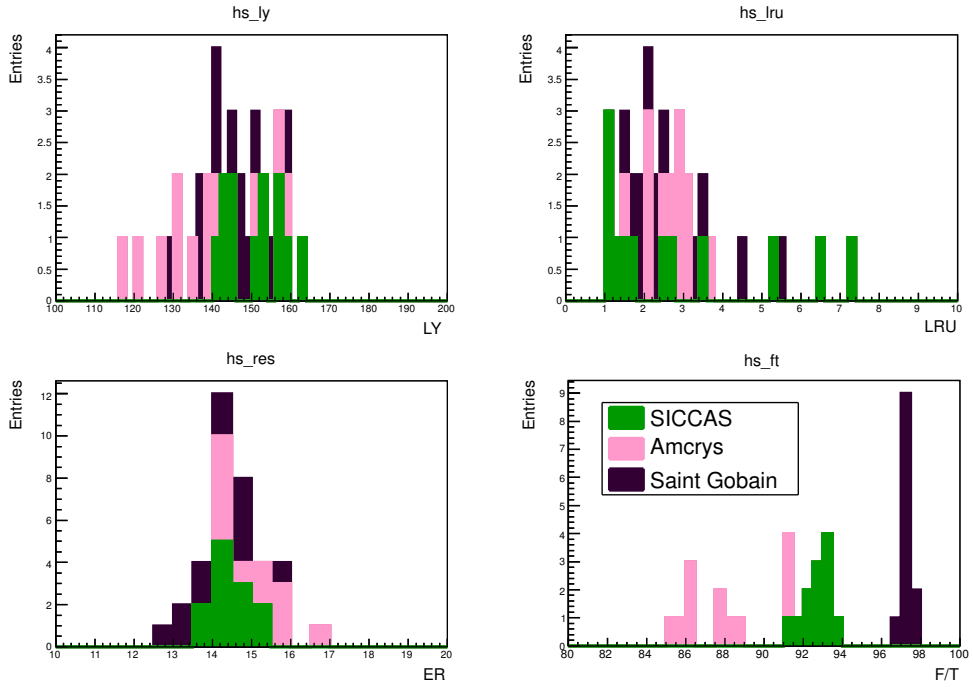

Figure 4: *Summary of the measurement performed at the crystal test station for the pre-production of un-doped CsI crystals. Distributions of: (top-left) LY, (top-right) LRU, (bottom-right), energy resolution, (bottom-left) F/T ratio.*

time minimizes the overall width of the Crystal+SiPM pulse height thus improving the pileup discrimination capability.

3.1 Neutron irradiation test of SiPMs at HZDR

In May 2016, an irradiation test has been performed at the EPOS source (HZDR, Dresden) with a flux of ∼1 MeV neutrons. The experimental setup used is reported in Figure 7: a SiPM with a Silicon protection layer (SPL) was located over the source in a place where no dose from γ's was present. The SiPM was monitored both in current and in charge while illuminated with an UV led. To maintain the SiPM temperature as stable as possible, the irradiated SiPM was connected to a Peltier cell, with the hot side glued to a cooling system. The SiPM temperature was monitored using a PT1000. In order to precisely monitor the input led light, a UV extended photomultiplier has been illuminated with the same led pulse by means of a split fiber and placed in a safe region located 2 m far away from the source. The SiPM was biased at $V_{op} = 54.9$ V. The total neutron fluency absorbed by the SiPM in five days was $\sim 5.5 \times 10^{11}$ n_{1MeV}/cm^2, that is three times the flux expected in the hottest Mu2e region in three years of running. In Fig. 8, the irradiation results are shown as a function of the integrated flux. The signal peak decreased from ∼650 mV to ∼350 mV, due to the residual temperature variation. A rising behaviour of the SiPM leakage current, from 60 μA up to 12 mA, is instead clearly visible.

In order to study the SiPM properties as a function of its temperature, the SiPM irradiated at EPOS and one not irradiated SiPM have been tested in a vacuum chamber at $\sim 10^{-4}$ mbar

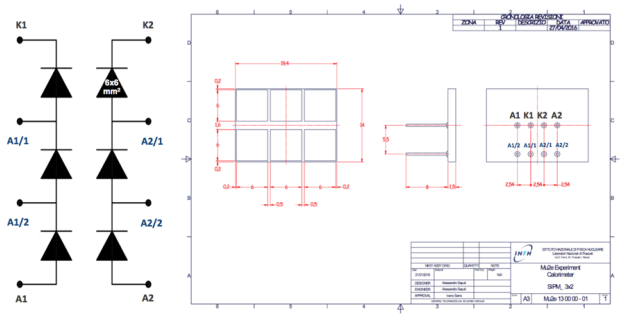

Figure 5: *Sketch and schematic structure (from left to right) of the front, lateral and back side views of the Mu2e SiPMs.*

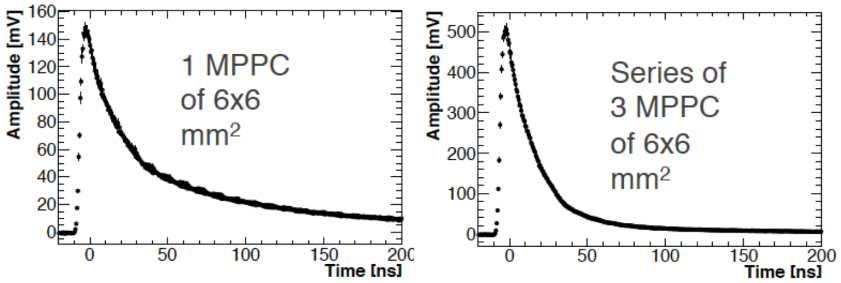

Figure 6: *Left: signal width of a single* (6×6) mm^2 *SiPM. Right: Signal width of a series of three* (6×6) mm^2 *SiPMs.*

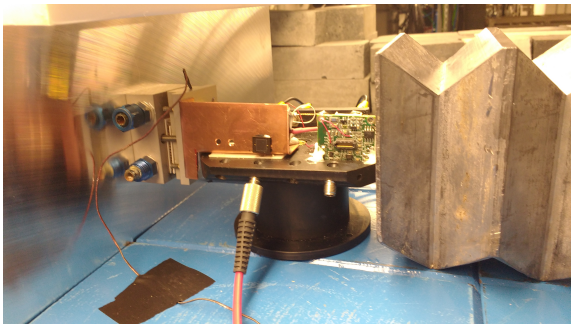

Figure 7: *Experimental setup used at HZDR.*

and cooled by means of a cascade of two Peltier cells. The SiPM temperature was monitored by a PT1000 sensor. A UV LED was illuminating directly the sample inside the chamber. Results from this test ensure to reach the Mu2e requirements on the maximum SiPM current by keeping its temperature at $T < 0$ °C.

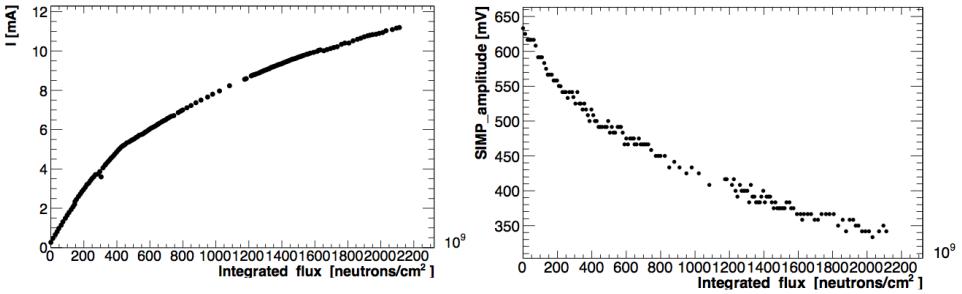

Figure 8: *Variation of SiPM leakeage current (left) and signal amplitude (right) as a function of the integrated flux.*

3.2 Determination of Mean Time To Failure for the Mu2e SiPMs

The Mean Time To Failure, MTTF, is the mean time to the first failure under specified experimental conditions. It is one way used to evaluate the reliability of pieces of hardware or other technology. In may 2016 a first MTTF determination using four (6×6) mm^2 FBK SiPMs have been performed. The SiPMs were put in a box maintained at 50 °C using Peltier cells and pulsed every 300 s with a UV led. Observing no deads in two months for 4 SiPMs corresponds to a measured MTTF of $> 0.26 \times 10^6$ hours. This value is evaluated as follows: MTTF $> 0.5\times N_{hours}\times AF\times N_{SiPM}$ where N_{hours}= 2190, N_{SiPM}=5 and the Acceleration Factor (AF) can be extracted from the Arrhenius equation:

$$AF = exp\left[\frac{E_a}{k}\left(\frac{1}{T_{use}} - \frac{1}{T_{stress}}\right)\right] \quad (2)$$

In November 2016, a new MTTF test has started for the pre-production of Mu2e SiPMs. 15 sensors from three different vendors (Advansid, Hamamatsu and SensL) will be kept under test until middle of March 2017 to reach an MTTF value of 0.6×10^6 hours. The test is performed keeping the SiPMs in a light tight box at 50 °C for three months. The dark current is measured once a day by a picoammeter and the response to a blue led is acquired every two minutes. The new experimental setup is show in Fig. 9.

4 Calorimeter Mechanics

We tailored the calorimeter mechanical structure around the best ideal layout for the crystals as obtained by simulation to maximize the acceptance for conversion electrons. The adopted solution is to pile up the crystals in a self-standing array organized in consecutive staggered rows. The active area of the Mu2e calorimeter consists of two annuli with an inner radius of 375 mm and an outer radius of 657 mm containing a number of 674 staggered scintillating crystals with a square prism shape $(34 \times 34 \times 200)$ mm^3, each one wrapped with a 150 μm thickness reflective sheet (Tyvek) for a total weight of 700 kg. Each annulus has an inner radius of 336 mm, an outer radius of 910 mm including all the electronics crates.

Fig. 10 is an exploded view of all the elements composing each annulus. As shown, each crystal array is supported by two coaxial cylinders. The inner cylinder must be as thin and light as possible in order to minimize the passive material in the region where spiraling background

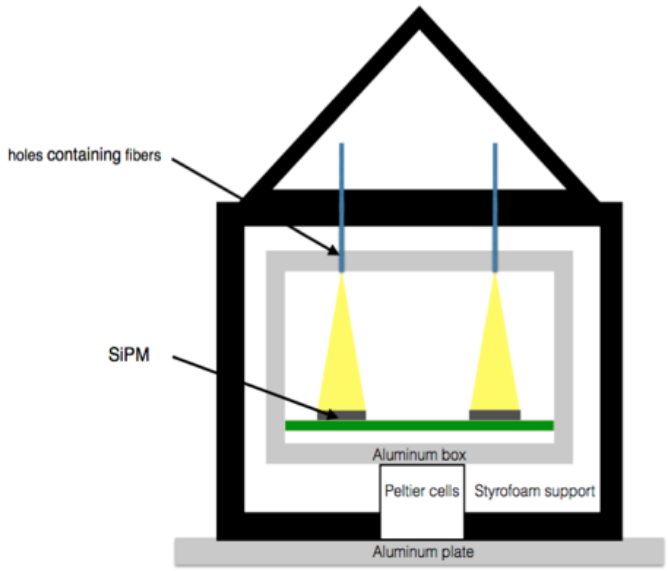

Figure 9: *Sketch of the new experimental setup used for the MTTF test of the pre-production SiPMs.*

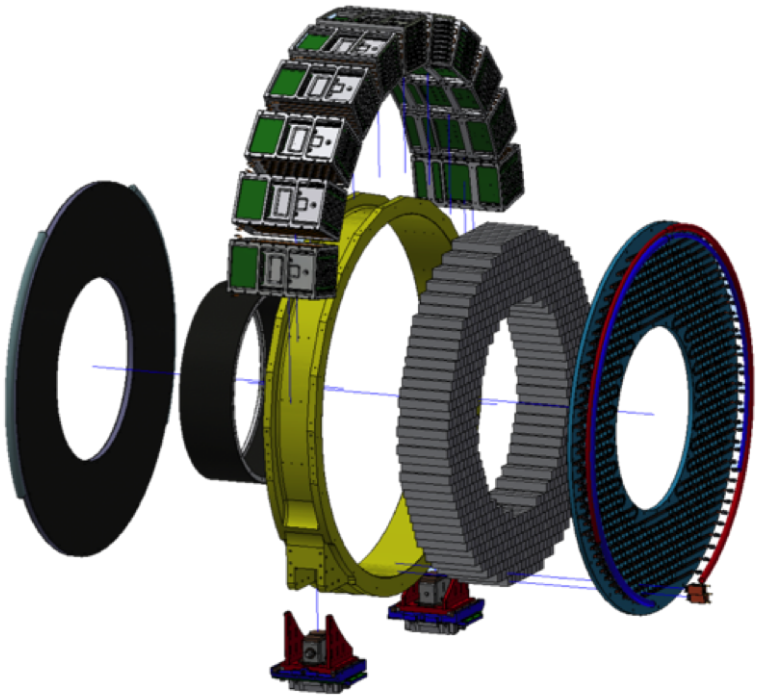

Figure 10: *Exploded view of the calorimeter mechanical structure.*

electrons are concentrated. The outer cylinder is as robust as required to fully support the load of the crystals. Each disk has two cover plates. The plate facing the beam is made of carbon fiber to minimize the degradation of the electron energy reaching the active area, while the back plate can be very robust. The back plate will also serve as support for the SiPMs, for the front-end electronics and for the cooling pipes.

The crystal arrangement is self-supporting, with the load carried primarily by the outer ring. A catenary structure resembling a Roman arch is constructed to reduce the overall load on the inner cylinder. The mechanical properties of the crystals are critical for this type of configuration. These include the Young modulus, tensile modulus, Poisson ratio (or torsional modulus of elasticity), yield strength and ultimate strength. A Finite Element Model, using the crystal properties as input, has been constructed to optimize the design of the structural components and to verify that the crystals could be piled up and sustain their own weight. The boundary conditions of this layout are fixed and the structural analysis has been used to verify displacements and deformations of the various components. We have built a first prototype of the outer cylinder and the supporting feet that integrate X-Y adjustment mechanism. The mock-up prototype is shown in Figure 11.

Figure 11: *Full size mock-up of the calorimeter mechanical structure.*

The back plate will be built by plastic material with good outgassing properties, either Peek or Zedex. It provides support for the FEE electronics and SiPM holders and hosts the cooling pipes to dissipate the power of the electronics and cool down the sensors. A readout unit is composed of a crystal, two SiPMs and two AMP-HV chips. The back plate will provide visual access to each crystal. The front plate will be made of carbon fiber and will embed the piping for running the

source calibration fluid.

5 Electronics

The overall scheme for the calorimeter readout electronics is shown in Fig. 12.

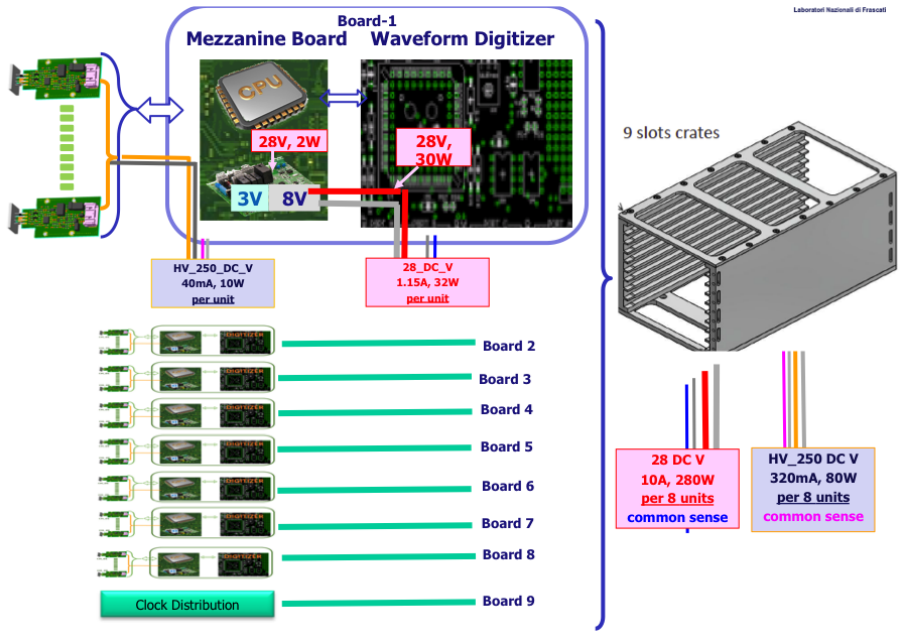

Figure 12: *General layout of the electronics scheme: from FEE attached to the SiPMs to the Mezzanine and Waveform Digitizer boards.*

The FEE consists of two discrete and independent chips (Amp-HV), for each crystal, directly connected to the back of the SiPM pins. These provide the amplification and shaping stage, a local linear regulation of the bias voltage, the monitoring of current and temperature on the sensors and a pulse test. Each disk is subdivided into 34 similar azimuthal sectors of 20 crystals. Groups of 20 Amp-HV chips are controlled by a dedicated mezzanine board (MB), where an ARM controller distributes the LV and the HV reference values, while setting and reading back the locally regulated voltages. Groups of 20 signals are sent in differential way to a digitizer module (WD) where they are sampled and processed before being optically transferred to the DAQ system. The Detector Control System parameters read-out/set by the MB are passed via I2C to the WD that then communicates them to the DCS system through an optical link. The Amp-HV is a multi-layer double-sided discrete component chip that carries out the two tasks of amplifying the signal and providing a locally regulated bias voltage, thus significantly reducing the noise loop-area. The two functions are each independently executed in a single chip layer, named the Amp and HV sides, respectively. The AMP-HV chips are asked to provide: (i) two settable amplification values (10, 20) with low noise, (ii) a signal rise time comparable with 3 to 5 times the WD sampling time for good time resolution and (iii) a short falling time to improve pileup rejection, (iv) a low detection threshold below the MeV level, (v) a high precision and stability in regulating and keeping the operation voltage (vi) a capability of operating in a rate environment of 500 kHz/channel without diminishing its gain, shape and pileup rejection capability, (vii) a stable output regardless to the average current due to Idark from the SiPM or radiation induced noise in the crystals assuming

those to be contained below the mA, (viii) a stability to the response also in presence of 500 kHz beam flash signals and, finally, (ix) a low power consumption. Moreover, the AMP-HV chip has been added with three independent monitoring capabilities: (M1) the readout of the SiPM temperature, (M2) the readout of the current drawn in the two series and (M3) the generation of a pulse signal to test the amplifier gain. The three latter monitoring capabilities, as well as the readout and setting of the operation voltages, are controlled by means of I2C.

The development of the Amp-HV chip has been done by the LNF Electrical Design Department (SEA). This final design has been built upon a long R&D phases carried out for the different calorimeter prototyping stages: forty prototypes were built during 2013 and have been used for testing a LYSO matrix readout with APD, 10 prototypes were build in 2015 for the test of BaF_2 readout with solar blind APDs and finally 150 prototypes (version-0) are now in preparation for the module-0 assembly with CsI and custom Mu2e SiPMs. In Fig. 13 a picture of the first prototype is shown. The chip is constituted by a 8 layers PCB of compact dimension 30×60 mm^2.

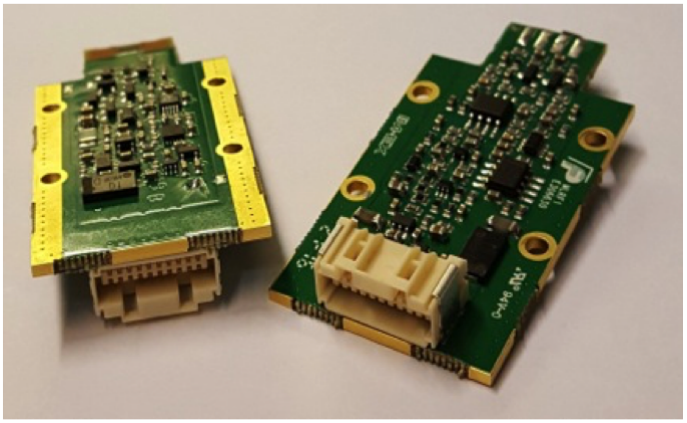

Figure 13:

On the Top layer, there are located the preamplifier, the shaper filter and a differential buffer as well as the digital logic (DAC and ADC) to set and read back the bias voltage on the local regulator, read the local temperature and create a pulse signal. On the bottom layer, there is the local regulator for the bias voltage. The regulator is in linear technology, it can provide a maximum of 2 mA at 200 V and is fully programmable by remote.

6 Acknowledgments

The authors are grateful to many people for the help provided during 2016, in particular the mechanical shop for their support in the preparation of the mockup and for the test of crystals under load. A great help was directly provided by T. Napoletano for the 3D printing of many calorimeter details and for the measurement of dimension and shape of the CsI crystals. Moreover, we are in debt with D. Alesini and the LNF vacuum department for the outgassing characterization of many of the calorimeter components. These tests were not possible without the expertize and skills of V.Lollo and S.Bini: a special direct thank goes to the two of them.

7 List of Conference talks/prices by LNF authors in Year 2016

Talks:

1. R. Donghia, "L'esperimento Mu2e", XV Incontri di Fisica delle Alte Energie (IFAE 2016), Genova, 30 March - 1 April 2016, Italy.

2. R. Donghia, "Design, R&D and status of the crystal calorimeter for the Mu2e experiment", XVIII LNF Spring School Bruno Touschek in Nuclear, Subnuclear and Astroparticle Physics, LNF, 9-13 May 2016.

3. M. Martini, "Design, status and test of the Mu2e crystal calorimeter", CALOR 2016, 15-20 May 2016, Daegu, Republic of Korea.

4. E. Diociaiuti and R. Donghia, "Study of radiation hardness of undoped CsI crystals and Silicon Photomultipliers for the Mu2e calorimeter", poster, CALOR 2016, 15-20 May 2016, Daegu, Republic of Korea.

5. I. Sarra, "The Mu2e Experiment at Fermilab", 22nd International Symposium on Particles, Strings and Cosmology (PASCOS 2016), July 10-16 2016, Quy Nhon, Vietnam.

6. E. Diociaiuti, "Characterization of crystal and SiPM of the Mu2e electromagnetic calorimeter", Società Italiana di Fisica, 102° Congresso Nazionale (SIF 2016), Padova 26-30 September 2016, Italy.

7. F. Happacher, "The Mu2e Experiment at Fermilab", New Trends in High-Energy Physics, 2-8 October 2016, Budva, Becici, Montenegro.

8. E. Diociaiuti, "Irradiation study of UV Silicon Photomultipliers for the Mu2e Calorimeter", poster, 14th Topical Seminar on Innovative Particle and Radiation Detectors (IPRD16) 3-6 October 2016, Siena, Italy.

Publications:

1. N. Atanov *et al.*, "Measurement of time resolution of the Mu2e LYSO calorimeter prototype", Nucl. Instrum. Meth. A 812 (2016) 104.

2. M. Angelucci *et al.*, "Longitudinal uniformity, time performances and irradiation test of pure CsI crystals", Nucl. Instrum. Meth. A 824 (2016) 678.

3. N. Atanov *et al.*, "Design and status of the Mu2e electromagnetic calorimeter", Nucl. Instrum. Meth. A 824 (2016) 695.

4. N. Atanov *et al.*, "Energy and time resolution of a LYSO matrix prototype for the Mu2e experiment", Nucl. Instrum. Meth. A 824 (2016) 684.

5. R. Donghia *et al.*, "Performance study of single undoped CsI crystals for the Mu2e experiment", Il Nuovo Cimento 39 C (2016) 276.

6. R. Donghia *et al.*, "Design, R&D and status of the crystal calorimeter for the Mu2e experiment", Frascati Physics Series Vol. LXIII (2016) 37.

7. N. Atanov *et al.*, "The calorimeter of the Mu2e experiment at Fermilab", JINST 12 (2017) C01061.

8. S. Baccaro *et al.*, "Irradiation study of UV Silicon Photomultipliers for the Mu2e calorimeter", JINST 12 C02022.

Mu2e Internal notes:

1. M. Cordelli *et al.*, "Measurement of the slow component for undoped CsI crystals", Mu2e-doc-6813, February 2016.